Layered $H_2Ti_6O_{13}$-Nanowires: A New Promising Pseudocapacitive Material in Non-Aqueous Electrolyte

Yonggang Wang, Zhensheng Hong, Mingdeng Wei,* and Yongyao Xia**

Layered $H_2Ti_6O_{13}$-nanowires are prepared using a facile hydrothermal method and their Li-storage behavior is investigated in non-aqueous electrolyte. The achieved results demonstrate the pseudocapacitive characteristic of Li-storage in the layered $H_2Ti_6O_{13}$-nanowires, which is because of the typical nanosize and expanded interlayer space. The as-prepared $H_2Ti_6O_{13}$-nanowires have a high capacitance of 828 F g^{-1} within the potential window from 2.0 to 1.0 V (vs. Li/Li^+). An asymmetric supercapacitor with high energy density is developed successfully using $H_2Ti_6O_{13}$-nanowires as a negative electrode and ordered mesoporous carbon (CMK-3) as a positive electrode in organic electrolyte. The asymmetric supercapacitor can be cycled reversibly in the voltage range of 1 to 3.5 V and exhibits maximum energy density of 90 Wh kg^{-1}, which is calculated based on the mass of electrode active materials. This achieved energy density is much higher than previous reports. Additionally, $H_2Ti_6O_{13}$//CMK-3 asymmetric supercapacitor displays the highest average power density of 11 000 W kg^{-1}. These results indicate that the $H_2Ti_6O_{13}$//CMK-3 asymmetric supercapacitor should be a promising device for fast energy storage.

1. Introduction

Supercapacitors, also known as electrochemical capacitors (ECs), are currently attracting intensive attention because they can provide energy density higher by orders of magnitude than dielectric capacitor, and greater power density and longer cycling ability than conventional rechargeable batteries.[1,2] Examples of envisioned large-scale application of supercapacitors are load-leveling in solar, wind, and other energy from regeneration braking in electronic vehicles (EVs).[1–3] Capacitance of supercapacitors mainly arises from surface reaction of electrode materials, including the surface charge separation at electrode/electrolyte interface (i.e., electrochemical double layered capacitive behavior) and surface faradic redox reactions (i.e., pseudocapacitve behavior).[1–3] Carbon materials with high surface area generally display electrochemical double layered capacitive behavior. Transition metal oxides or conductive polymers exhibit typical pseudocapacitve behavior. It also has been demonstrated that the pesudocapacitance of transition metal oxides or conductive polymers is much higher than the electrochemical double layered capacitance of carbon materials.[1–3]

Although the power density of supercapacitors is much higher than that of conventional rechargeable batteries, their energy density is still lower than that of conventional rechargeable batteries. Nowadays, much research on supercapacitors is aimed at increasing energy density as well as lowering fabrication costs while using environmentally friendly materials. Some transition metal oxides, such as amorphous RuO_2 and IrO_2,[4–11] exhibit prominent properties as pseudocapacitive electrode materials. The highest value for specific capacitance reported for amorphous hydrated RuO_2 is 1580 g^{-1}.[6] However, despite the remarkable performance of this material, its high cost excludes it from wide application. On the other hand, some low-cost transition metal oxides and conductive polymers also exhibit electrochemical capacitance behavior to some extent,[12–23] whereas their capacitance is much lower than that of RuO_2. The key reason is that amorphous RuO_2 can storage charge not only on the out surface but also within the expanded interlayer space.[5] Accordingly, it should be the best choice for building high performance supercapacitor to develop low cost pseudocapacitive materials, which can storage charge both on the out surface and in the interlayer gap of crystalline structure. Certainly, this should be a great challenge because the redox reaction in the interlayer gap of crystalline structure of electrode materials is always coupled with ions diffusion within the crystalline structure. In other words, the charge storage in the interlayer gap of crystalline structure of electrode materials is always controlled by diffusion process. However, the typical character of pseudocapacitive behavior is not limited by the ions diffusion process. Accordingly, in order to realize the pseudocapacitive behavior in the interlayer gap of crystalline structure, electrode materials with both typical expanded interlayer space and nanosize should be designed and prepared. This is

Prof. Y. G. Wang, Prof. Y. Y. Xia
Department of Chemistry and Shanghai Key Laboratory of Molecular Catalysis and Innovative Materials
Institute of New Energy
Fudan University
Shanghai 200433, P. R. China
E-mail: ygwang@fudan.edu.cn; yyxia@fudan.edu.cn
Dr. Z. S. Hong, Prof. M. D. Wei
Institute of New Energy Technology and Nano-Materials and National Engineering Research Center for Chemical Fertilizer Catalyst
Fuzhou University
Fuzhou, Fujian 350002, P. R. China
E-mail: wei-mingdeng@fzu.edu.cn

DOI: 10.1002/adfm.201200766

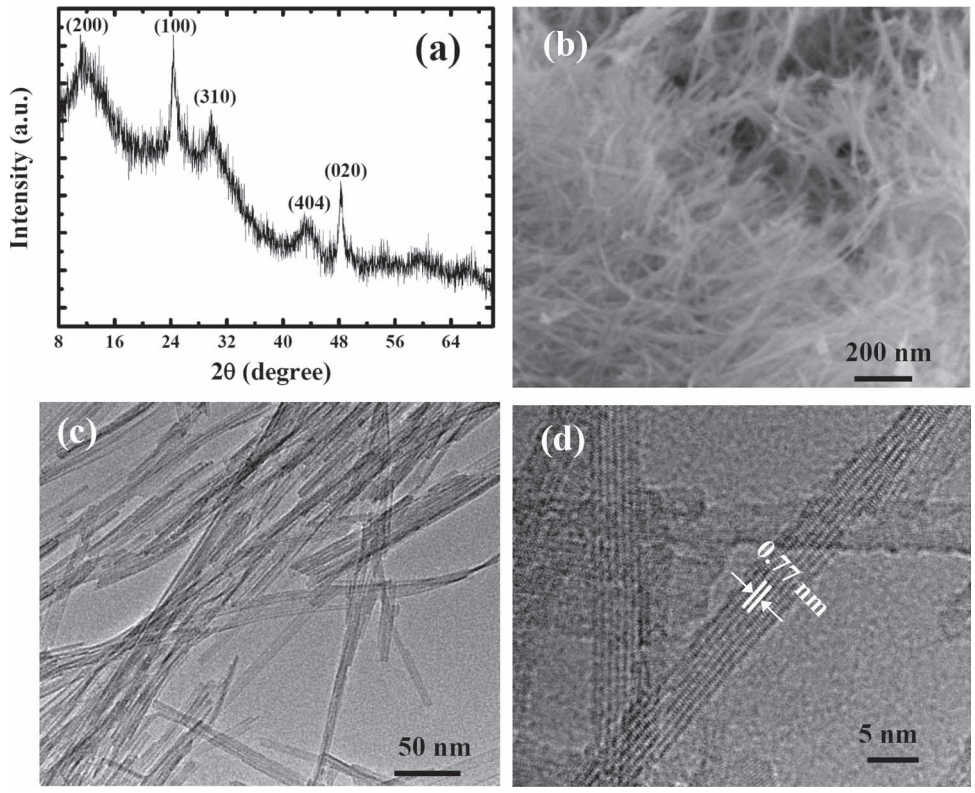

Figure 1. Titanate nanowires: a) XRD pattern, b) SEM image, and c,d) TEM and HRTEM images.

because expanded crystalline structure and nanosize can effectively facilitate ions diffusion and shorten diffusion length.

Besides enhancing capacitance of electrode materials, it also should be a promising approach for improving the energy density of supercapacitor to increase the operating voltage. It is well known that the max operating voltage of supercapacitor is limited by the stable potential window of electrolyte solution. For instance, supercapacitors using aqueous electrolyte can not achieve the max operating voltage that is higher than 2 V, owing to the narrow stable potential window of water. On the contrary, these supercapacitors using non-aqueous electrolyte can easily realize the max operating voltage of 3.0 V. However, up to date, pseudocapacitive behavior of electrode materials in non-aqueous electrolyte solution is rarely reported. Especially, almost all of transitional metal oxides, e.g., RuO_x, IrO_x, MnO_x, CoO_x, NiO_x, etc., display their pseudocapacitive behavior in aqueous electrolyte with various pH values.[12–23] Thereby, it is also very necessary to develop electrode materials with typical pseudocapacitive behavior in non-aqueous electrolyte.

In present work, we successfully prepared layered $H_2Ti_6O_{13}$-nanowires through a facile hydrothermal method followed with an acid treatment, and investigated their charge storage characteristic in non-aqueous electrolyte including Li-ions by various electrochemical measurements. Typical nanosize combining with the expanded interlayer result in the pseudocapacitive characteristic of Li-storage within the layered titanate nanowires in non-aqueous electrolyte. The as-prepared $H_2Ti_6O_{13}$-nanowires exhibit a high capacitance of 828 F g^{-1} within the potential window from 2.0 to 1.0 V (vs. Li/Li^+), and is a promising negative electrode for supercapacitor. Finally, an asymmetric supercapacitor which is based on a negative electrode of $H_2Ti_6O_{13}$ nanowires and a positive electrode of ordered mesoporous carbon (CMK-3) was fabricated. The achieved energy density of the asymmetric supercapacitor is as high as 90 Wh kg^{-1}.

2. Results and Discussion

2.1. Character of $H_2Ti_6O_{13}$-Nanowires

The character of the as-prepared titanate nanowires is given in **Figure 1**. It can be revealed from the XRD pattern that the as-prepared material can be indexed to the structure of layered titanate of $H_2Ti_6O_{13}$ (Figure 1a).[24] Figure 1b–d depicts the SEM image and TEM image of the as-prepared $H_2Ti_6O_{13}$-nanowires. As shown in Figure 1b, many $H_2Ti_6O_{13}$-nanowires agglomerate together to form a network structure. The typical size of $H_2Ti_6O_{13}$-nanowires is 5–7 nm in diameter and 50–150 nm in length (Figure 1c). Figure 1d shows the high solution TEM (HSTEM) image of $H_2Ti_6O_{13}$-nanowires, further confirming the nanowires shape with a typical diameter size of 5 nm. HRTEM image also reveals that the interlayer spacing of layered titanate is ca. 0.77 nm, corresponding to the distance between (200) planes. The unique nanostructure and typical nanosize of the prepared $H_2Ti_6O_{13}$ can effectively shorten the

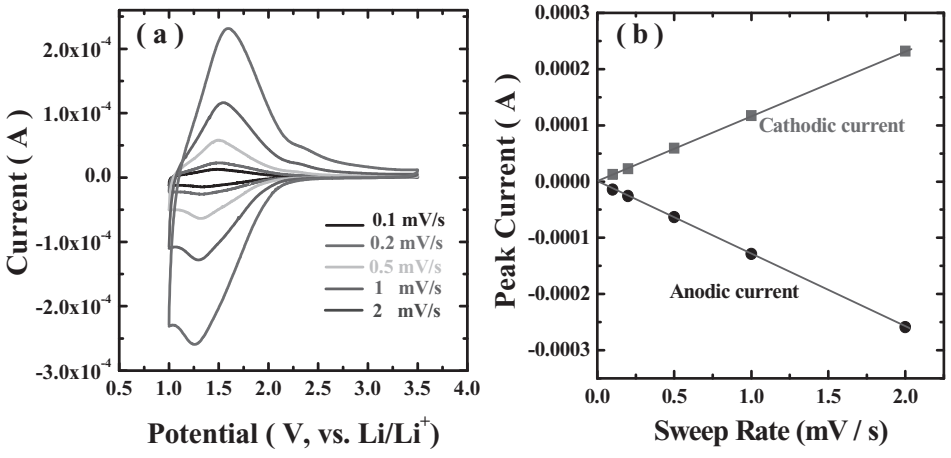

Figure 2. CV curves at various sweep rates (a) and the relationship between peak current (i_p) and sweep rate of titanate nanowires (b).

ion diffusion length on charge/discharge process. Furthermore, the expanded interlayer space (ca. 0.77 nm) could facilitate the Li-intercalation/deintercalation process. These will be confirmed by electrochemical investigations. The specific surface area of the as-prepared $H_2Ti_6O_{13}$-nanowires is 330m^2 g^{-1}. This large surface area can much enhance electrode/electrolyte interface, and thus increase the surface redox reaction which is not controlled by the diffusion process.

Cyclic voltammetry (CV) experiments carried out at various sweep rates were used to examine the redox processes occurring in the as-prepared $H_2Ti_6O_{13}$-nanowires. As shown in **Figure 2**a, a couple of redox peaks are observed between 2.0 V and 1.0 V vs. Li/Li$^+$. These peaks correspond to the intercalation and deintercalation of Li-ion and can be represented by the following equation:

$$H_2Ti_6O_{13} + xLi^+ + xe^- \leftrightarrow Li_xH_2Ti_6O_{13} \quad (1)$$

The voltammetric response of electrode active material at various sweep rates can be summarized according to:[25–27]

$$i = av^b \quad (2)$$

in which the measure current (i) at a specific potential obeys a power law relationship with the potential sweep rate (v). It is well known that the cation intercalation of battery behavior is a diffusion controlled process, and thus the current flow at any given potential is expected to vary with the square root of the sweep rate ($b = 0.5$) according to:

$$i = nFAC^* D^{1/2} v^{1/2} (\alpha nF/RT)^{1/2} \pi^{1/2} \chi(bt) \quad (3)$$

where C^* is the surface concentration of the electrode material, α is the transfer coefficient, D is the chemical diffusion coefficient, n the number of electrons involved in the electrode reaction, A is the surface area of the electrode material, F is the Faraday constant, R is the molar gas constant, T is the temperature, and the function $\chi(bt)$ represents the normalized current.[27] According to Equation (3), the current (i) of battery behavior at any given potential should be the function of both potential sweep rate (v) and sweep time (t). At a specific sweep time (or a specific potential), the current (i) is only the function of sweep rate (v). Accordingly, for battery behavior, the relationship between peak current (i_p) and sweep rate (v) can be presented by $i_p = av^{0.5}$ ($b = 0.5$). In contrast to battery behavior, typical capacitive behavior is not diffusion controlled, and thus the current (i) should vary linearly with the sweep rate ($b = 1$) according to:[25–27]

$$i = C_d Av \quad (4)$$

where C_d represents the capacitance and A is the surface area of active materials.[27] Pseudocapacitive behavior of active material arises from the surface faradic redox reactions, and is not controlled by diffusion process. Because the surface faradic redox reactions only occur in a specific voltage region, pseudocapacitive behavior also displays obvious redox peaks on CV test. Accordingly, the peak current (i_p) for pseudocapacitive behavior should vary linearly with the sweep rate ($b = 1$ or $i_p = C_dAv$). Figure 2b gives the voltammetric response of the as-prepared $H_2Ti_6O_{13}$-nanowires at various sweep rates. It can be detected from Figure 2b the peak current (i_p) increases linearly with the increase of sweep rate. The linear relationship of i_p vs. v ($b = 1$) clearly demonstrates the pseudocapacitive characteristic of lithium storage in the as-prepared $H_2Ti_6O_{13}$-nanowires.

In order to further confirm the pseudocapacitive characteristic of lithium storage, electrochemical impedance spectroscopic (EIS) analysis of the as-prepared $H_2Ti_6O_{13}$ at a selected discharge depth was conducted. Prior to EIS measurement, $H_2Ti_6O_{13}$ nanowires electrode was discharged to 1.5 V vs. Li/Li$^+$ and hold at this potential for 3 h to reach equilibrium (see **Figure 3**a). Then, EIS measurement was performed at this potential (1.5 V vs. Li/Li$^+$) in the frequency range 10^6–0.01 Hz with AC signal amplitude of 5 mV. The obtained Nyquist plot (Z'' vs. Z') is given in Figure 3b. The Nyquist plot typically consists of a high frequency semicircle and a low frequency spike. Typically, the high frequency semicircle is associated with these resistances: the internal resistance of electrode, interface resistance and charge transfer resistance. In the low frequency region, typical linear shape of Nyquist plot can be observed where the slope gradually changes from 45° to 90° with decrease of ac frequency, indicating that the Li-intercalation in the as-prepared $H_2Ti_6O_{13}$-nanowires is not controlled by the diffusion process.[1,27] In other words, this result clearly demonstrates that the as-prepared $H_2Ti_6O_{13}$-nanowires are able to accommodate Li$^+$ through pseudocapacitive processes. After EIS measure the $H_2Ti_6O_{13}$ nanowires electrode was further discharged to 1.0 V.

In addition to these electrochemical investigations, XRD measurement should be a direct method to confirm pseudocapacitive behavior. For pseudocapacitive behavior, the charge storage mainly takes place on (or near) the surface of

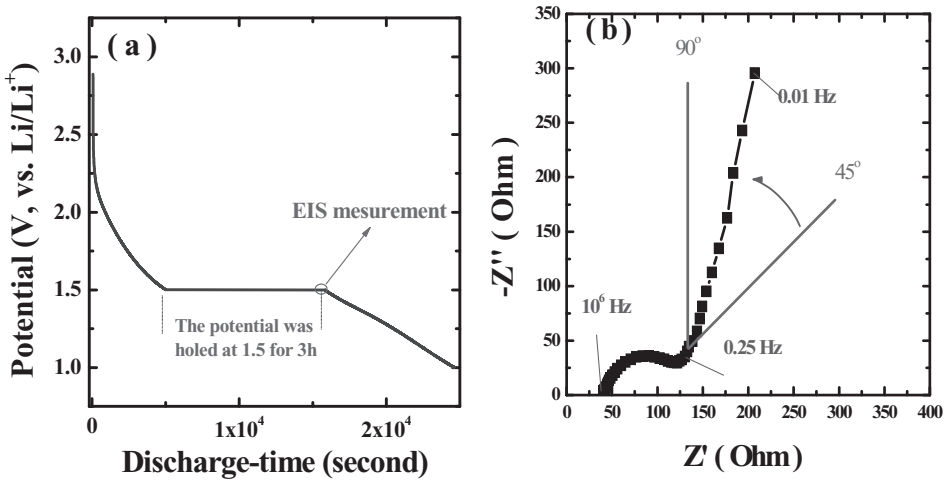

Figure 3. a) Discharge curve and b) Nyquist plot obtained from EIS measurement of titanate nanowires.

active materials, which would not lead the obvious crystalline parameters change of active materials. Thereby, we employed XRD technology to characterize the Li-intercalated $H_2Ti_6O_{13}$-nanowires. After full Li-intercalation (or discharged to 1.0 V with a current density of 30 mA g^{-1}, see **Figure 4**a), the $H_2Ti_6O_{13}$ electrode was disassembled in the argon-filled glove box, and then the Li-intercalated $H_2Ti_6O_{13}$ electrode was transferred for assembly in an ex situ XRD cell in which thin Al film was used as a window (detailed information for this experiment is given in Supporting Information Figure S1). Figure 4b gives the XRD pattern of Li-intercalated $H_2Ti_6O_{13}$ electrode. The XRD pattern obtained at the same measurement condition of fresh $H_2Ti_6O_{13}$ electrode (without Li-intercalation) is also given in Figure 4b for comparison. It can be observed from Figure 4b that the XRD pattern of Li-intercalated $H_2Ti_6O_{13}$ electrode is almost as same as that of fresh $H_2Ti_6O_{13}$ electrode. It also should be noted that the additional diffraction peaks at around 18° arises from the binder (PTFE) of $H_2Ti_6O_{13}$ electrode. A $H_2Ti_6O_{13}$ composite electrode includes binder (polytetrafluoroethylene, PTFE), active material ($H_2Ti_6O_{13}$-nanowires) and carbon additive (acetylene black). This result from Figure 4b clearly demonstrates that the Li-intercalation does not result in obvious crystalline parameters change of $H_2Ti_6O_{13}$, indicating the pseudocapacitive characteristic of Li-storage.

Figure 5a gives the charge/discharge curves of the as-prepared $H_2Ti_6O_{13}$-nanowires within the potential window from 3.5 V to 1.0 V (vs. Li/Li^+) at different current densities. As shown in Figure 5a, the as-prepared $H_2Ti_6O_{13}$-nanowires exhibit slope charge/discharge curve within the potential region of 2.0 V to 1.0 V, which is consistent with the CV tests. The specific capacitance of the prepared $H_2Ti_6O_{13}$-nanowires can be calculated according to Equation (5):

$$C = \frac{I \times t}{m \times \Delta V} \tag{5}$$

in which C is the specific capacitance (F g^{-1}), I is charge-discharge current, ΔV is 1 V (As shown in Figure 5a, $H_2Ti_6O_{13}$-nanowires exhibit their capacity in the region of 2.0 V to 1.0 V),

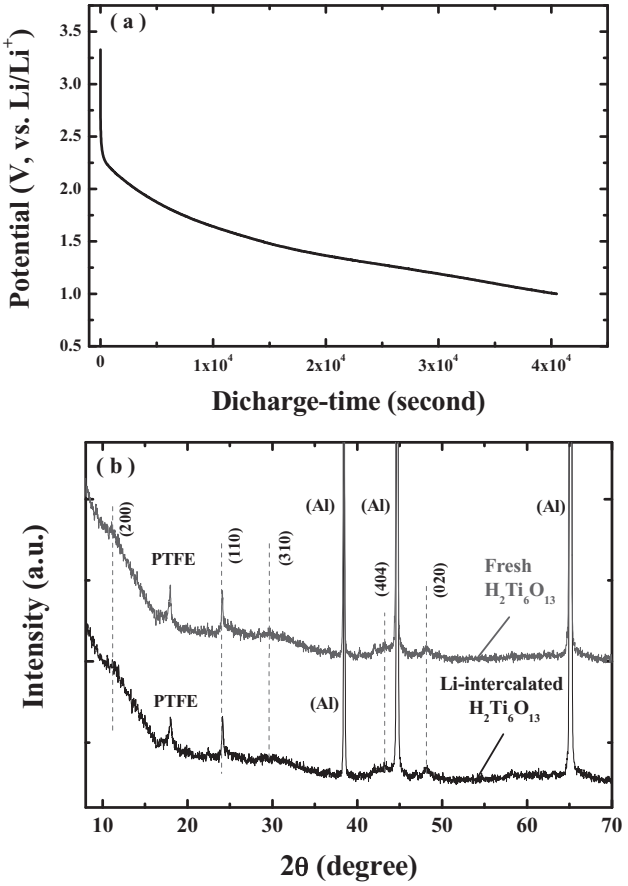

Figure 4. a) The discharge curve of $H_2Ti_6O_{13}$-nanowired based electrode and b) the XRD patterns of Li-intercalated $H_2Ti_6O_{13}$ electrode and fresh $H_2Ti_6O_{13}$ electrode.

and m is the mass of active material within the electrode. The calculated results from Equation (5) are summarized in Figure 5b. As shown in Figure 5b, the as-prepared $H_2Ti_6O_{13}$-nanowires

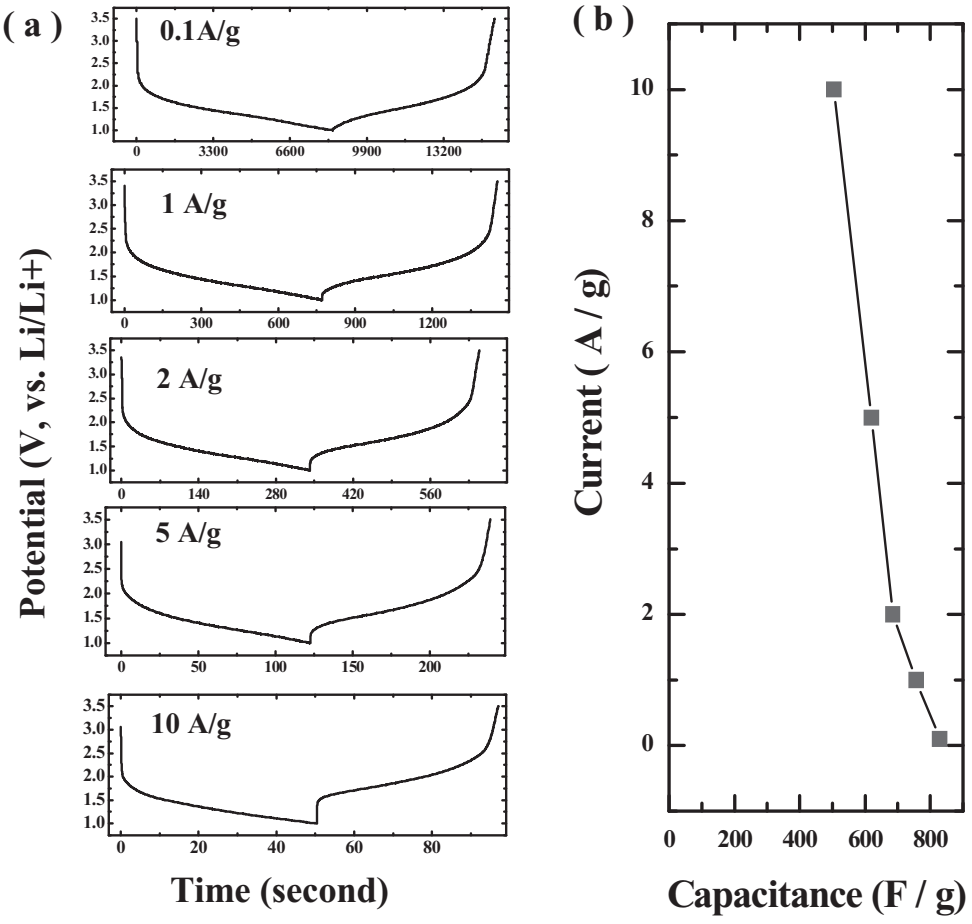

Figure 5. a) Charge/discharge curve (V vs. time) of titanate nanowires and b) calculated capacitance (F/g) at different current densities.

exhibit a capacitance of 828 F g^{-1} at a charge/discharge current density of 0.1 A g^{-1}. When the current density is increased to 2 A g^{-1}, the as-prepared $H_2Ti_6O_{13}$-nanowires display a capacitance of 684 F g^{-1}. Even at much higher rate (10 A g^{-1}), the prepared material still keeps a capacitance of 504 F g^{-1}. This clearly indicates that as-prepared $H_2Ti_6O_{13}$-nanowires are of perfect rate performance.

The results given in Figure 2, 3, 4 and 5 demonstrate that the as-prepared $H_2Ti_6O_{13}$-nanowires are able to accommodate Li^+ through pseudocapacitive processes. The pseudocapacitive behavior of the $H_2Ti_6O_{13}$-nanowires arises from their unique structure. Firstly, the interlayer space (ca. 0.77 nm) of the as-prepared $H_2Ti_6O_{13}$-nanowires is wider than the interlayer space (or tunnel size) of conventional Li-intercalation compounds, which ensures the fast mobility of Li-ions. Secondly, typical size of $H_2Ti_6O_{13}$-nanowires is only 5–7 nm, which effectively shortens the diffusion length. Finally, the large surface area (330 m^2g^{-1}) arising from the nanosize and nanostructure much enhances the surface redox reaction and reduces the practical current density (A cm^{-2}). It should be noted that up to present, the electrode material with pseudocapacitive performance in organic (or non-aqueous) electrolyte solution is still rarely reported. **Table 1** summarizes the previous reports about the pseudocapacitive performance of transition metal oxides or conductive polymers. As shown in Table 1, all of these transition metal oxides or conductive polymers display their pseudocapacitive behavior in aqueous electrolyte solution with limited stable potential window. Compared with these previous metal oxides or conductive polymers, the advantages of the as-prepared $H_2Ti_6O_{13}$-nanowires include i) the capacitance of the as-prepared $H_2Ti_6O_{13}$-nanowires is as high as 828 F g^{-1}; ii) $H_2Ti_6O_{13}$ is low cost in comparison with these expensive transition metal oxides (e.g., RuO_x or IrO_x); and iii) the as-prepared $H_2Ti_6O_{13}$ should be a promising negative electrode material for supercapacitor because its operating potential window (2.0 to 1.0 V vs. Li/Li^+ or –1.0 to –2.0 V vs. NHE) is much lower than that of conventional transition metal oxides and conductive polymers.

2.2. Asymmetric Supercapacitor Based $H_2Ti_6O_{13}$-Nanowires and CMK-3

As mentioned above, the as-prepared $H_2Ti_6O_{13}$ nanowires should be a promising negative electrode material for supercapacitor. In order to further investigate this advantage,

Table 1. Electrolyte solutions and operating potential windows of different pseudocapacitive materials.

Materials	Electrolyte Solutions	Operating Potential Windows	Ref.
RuO_2	H_2SO_4 aqueous solution	0–1.0 V (vs. NHE)[a)]	[4–10]
MnO_2	Na_2SO_4 or K_2SO_4 aqueous solution	0–1.0 V (vs. NHE)	[12–15]
V_2O_5	KCl aqueous solution	0–1.0 V (vs. NHE)	[16]
VN_xO_y	KOH aqueous solution	0– –1.0 V (vs. NHE)	[17]
NiO_x	KOH aqueous solution	0–0.6 V (vs. NHE)	[18,19]
Co_3O_4	KOH aqueous solution	0–0.6 V (vs. NHE)	[20,21]
$Co(OH)_2$	KOH aqueous solution	0–0.6 V (vs. NHE)	[22]
Polyaniline	H_2SO_4 aqueous solution	0–1 V (vs. NHE)	[23]
$H_2Ti_6O_{13}$	1 M $LiPF_6$ in EC/EDC	2.0–1.0 V (vs. Li/Li^+)	Present work
Nanowires		–1.0– –2.0 V (vs. NHE)	

[a)]NHE is Normal Hydrogen Electrode.

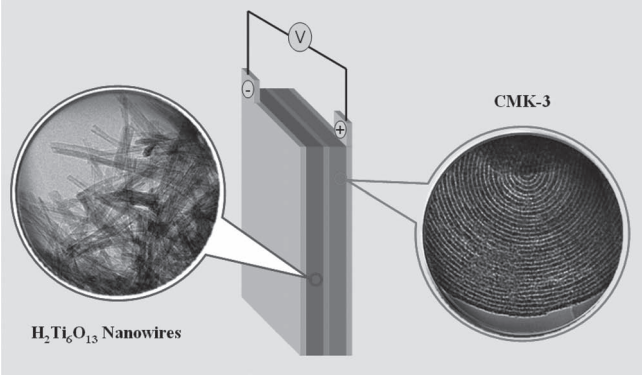

Figure 6. Schematic illustration of the fabricated asymmetric supercapacitor based on a positive electrode of CMK-3 and a negative electrode of $H_2Ti_6O_{13}$ nanowires in organic electrolyte solution (1 M $LiPF_6$ in EC/DEC).

we developed an asymmetric supercapacitor which is based on a negative electrode of $H_2Ti_6O_{13}$ nanowires and a positive electrode of ordered mesoporous carbon (CMK-3) in an organic electrolyte including Li-ions (see **Figure 6**). On charge process, anions from electrolyte are absorbed in porous structure of CMK-3 (positive electrode). At the same time, Li-ions from electrolyte are intercalated into the $H_2Ti_6O_{13}$-nanowires (negative electrode). Discharge reverses the charge process.

Figure 7 shows the charge/discharge curves of the individual composite electrode ($H_2Ti_6O_{13}$-electrode and CMK-electrode) vs. Li/Li^+ reference electrode, along with the voltage profile of the $H_2Ti_6O_{13}$//CMK-3 asymmetric supercapacitor at a current density of 0.2 A g^{-1}. As shown in Figure 7, the operating potential window of the negative electrode of $H_2Ti_6O_{13}$ is in the potential region from 2.0 to 1.0 V (vs. Li/Li^+). The positive electrode of CMK-3 is charged/discharged in the potential region from 3.0 to 4.5 V (vs. Li/Li^+), coupled with the absorption/desorption of anions. It can also be observed from Figure 7 that the $H_2Ti_6O_{13}$/CMK-3 asymmetric supercapacitor displays a slope voltage profile from 1.0 to 3.5 V, which is resulted from the potential difference between the positive electrode of CMK-3 and the negative electrode of $H_2Ti_6O_{13}$. **Figure 8** shows the charge/discharge curves of the $H_2Ti_6O_{13}$//CMK-3 asymmetry supercapacitor at different current densities. As shown in Figure 8, the $H_2Ti_6O_{13}$//CMK-3 asymmetric supercapacitor can finish charge or discharge within 30 s at the current density of 3A g^{-1}, indicating perfect power performance. The achieved high power of the fabricated asymmetric supercapacitor is owing to that both the negative electrode of $H_2Ti_6O_{13}$-nanowires and the positive electrode of CMK-3 have perfect rate ability (i.e., the performance of fast charge-discharge). The rate performance of the as-prepared $H_2Ti_6O_{13}$-nanowires has

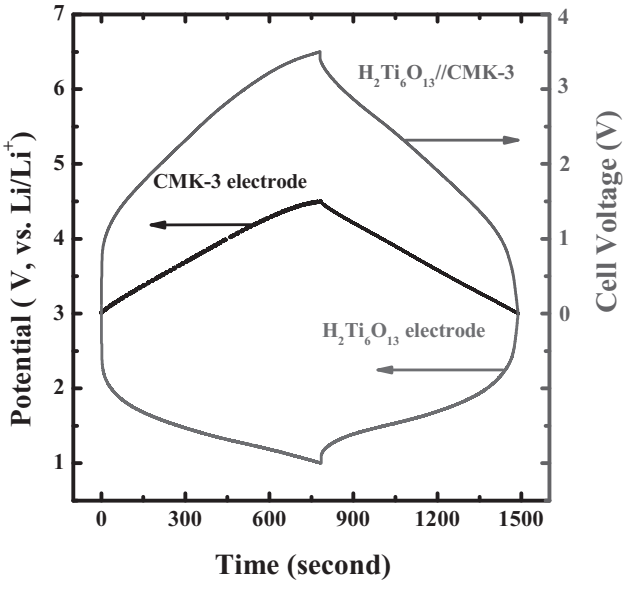

Figure 7. Charge/discharge curves of the individual composite electrode ($H_2Ti_6O_{13}$ and CMK-3) vs. Li/Li^+ reference electrode, along with the voltage profile of the $H_2Ti_6O_{13}$//CMK-3 asymmetric supercapacitor.

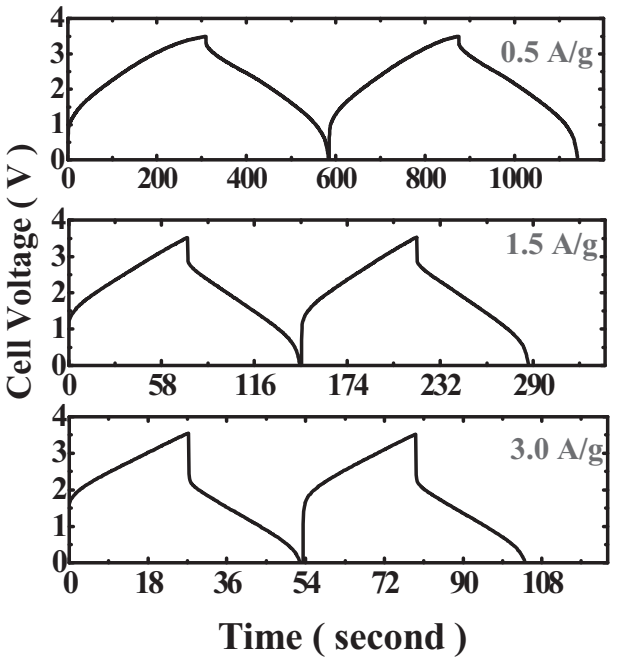

Figure 8. Charge/discharge curves of the $H_2Ti_6O_{13}$//CMK-3 asymmetry supercapacitor at different current densities.

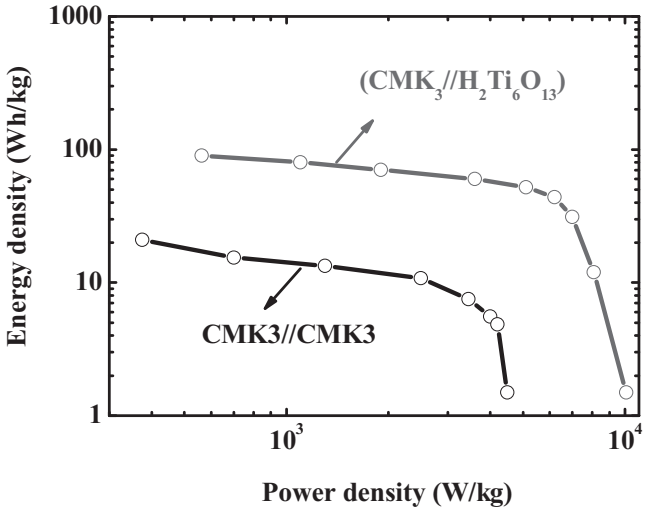

Figure 9. Ragone plots (energy density vs. power density) of the $H_2Ti_6O_{13}$//CMK-3 asymmetric supercapacitor and CMK-3//CMK-3 symmetric supercapacitor. The energy density (Wh kg^{-1}) and power density (W kg^{-1}) are only calculated based on the mass of electrode active materials.

been demonstrated by Figure 5. Furthermore, it also has been reported that ordered mesoporous carbons with a narrow distribution in the mesopore range and a uniform pore connection have much better electrochemical capacitive performance than conventional carbon materials, due to the mesopore channels and interconnections provide a more favorable path for penetration and transportation of ions.[28–31] In present manuscript, the electrochemical capacitive performance of the ordered mesoporous carbon is given in supporting information (see Supporting Information, Figure S2–4).

The Ragone plot (energy density vs. power density) of the $H_2Ti_6O_{13}$//CMK-3 asymmetric supercapacitor is given in **Figure 9**. The energy density values of the as-prepared supercapacitors were calculated by numerically integrating the discharge curves:

$$E = \int_{t_1}^{t_2} IV\mathrm{d}t = \frac{1}{2}C\,(V_1 + V_2)\,(V_1 - V_2) \tag{6}$$

where C is the capacitance (F g^{-1}) of supcapacitor and V_1 and V_2 are the end-of-charge voltage and the end-of-discharge voltage, respectively.

The average power density values of as-prepared supercapacitors were calculated according to Equation (6) and (7):

$$P = \frac{E}{t} \tag{7}$$

where t is the discharge time (s).

As shown in Figure 9, the achieved energy density and the max power density of the $H_2Ti_6O_{13}$//CMK-3 asymmetric supercapacitor are 90 Wh kg^{-1} and 11 000 W kg^{-1}, respectively. The Ragone plot of symmetric supercapacitor based CMK-3 (CMK-3//CMK-3) is also shown in Figure 9 for comparison. As shown in Figure 9, both energy density and power density of $H_2Ti_6O_{13}$//CMK-3 asymmetric supercapacitor is much higher than that of CMK-3//CMK-3 symmetric supercapacitor. The reason is that $H_2Ti_6O_{13}$//CMK-3 asymmetric supercapacitor can effectively utilize of the different potential windows between the two kinds of electrodes to increase the maximum operation cell voltage, resulting in an enhanced energy density (see Supporting Information Figure S5). Furthermore, the as-prepared $H_2Ti_6O_{13}$ nanowires are of high capacitance. From **Figure 10**, it can be detected that the capacitance retention of the $H_2Ti_6O_{13}$//CMK-3 asymmetric supercapacitor continuously

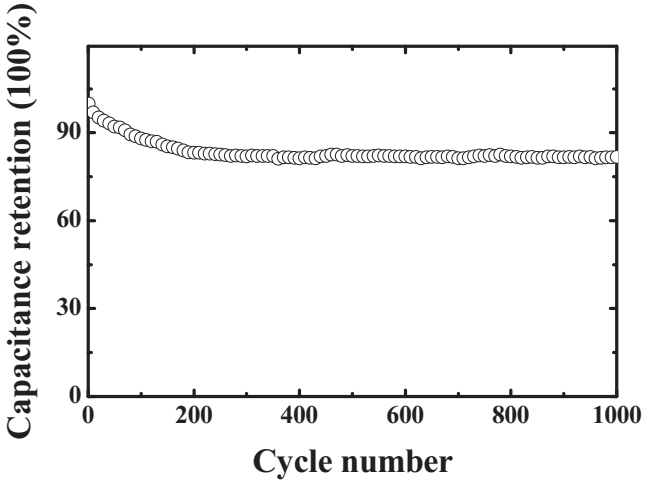

Figure 10. Cycling performance of the $H_2Ti_6O_{13}$//CMK-3 asymmetric supercapacitor tested with a current density of 1.5 A g^{-1}.

Table 2. Energy density and working voltage of various asymmetric supercapacitors.

Materials		Voltage	Energy density [Wh kg^{-1}]	Ref.
Positive electrode	Negative electrode			
$Ni(OH)_2$	Activated Carbon (AC)	0.5–1.5 V	40	[32]
$LiMn_2O_4$	AC	0.8–1.8 V	35	[33]
AC	$Li_4Ti_5O_{12}$	1.5–2.8 V	53	[34]
MnO_2	ACN	0–1.8 V	51.1	[35]
MnO_2	CNTs	0–1.5 V	12.5	[36]
CNTs	TiO_2-B	0–2.8 V	12.5	[38]
AC	V_2O_5	0–2.8 V	40	[39]
CMK-3	$H_2Ti_6O_{13}$	1.0–3.5 V	90	Present Work

reduces from initial cycle to 200th cycle, whereas the capacitance retention almost keeps at a constant value (80%) in the following cycling process, indicating good cycling ability.

It should also be noted that various asymmetric supercapacitors, such as activated carbon (AC)//$Ni(OH)_2$ system,[32] AC//$LiMn_2O_4$ system,[33] AC//$Li_4Ti_5O_{12}$ system,[34] AC(or CNTs)//amorphous MnO_2 system,[35–37] Carbon nanotubes (CNTs)//TiO_2 system,[38] AC/V_2O_5,[39] etc., have been reported recently. **Table 2** compares the performance of the $H_2Ti_6O_{13}$//CMK-3 asymmetric supercapacitor with previous reports about asymmetric supercapacitors. It can be found from Table 2 that the energy density of $H_2Ti_6O_{13}$//CMK-3 asymmetric supercapacitor is higher than previous reports. It should be noted that all of these energy density values (Wh kg^{-1}), given Table 2, are calculated based on the mass of electrode active materials.

3. Conclusions

In summary, the pseudocapacitive behavior of $H_2Ti_6O_{13}$-nanowires was investigated in non-aqueous electrolyte including Li-ions. The achieved results demonstrated that the as-prepared $H_2Ti_6O_{13}$-nanowires are of both high capacitance and low operating potential, and thus should be a promising negative electrode material for asymmetric supercapacitor. Thereby, the asymmetric supercapacitor based on as-prepared $H_2Ti_6O_{13}$-nanowires and CMK-3 can display simultaneously both high power and energy density, which is quite important for fast energy storage.

4. Experimental Section

Synthesis: Typically, 1 g of TiO_2 (anatase) was dispersed in a 50 mL of 15 M aqueous KOH solution. After stirring for 10 min, the resulting suspension was transferred into a Teflon-lined stainless steel autoclave with a capacity of 75 mL. The autoclave was kept at 170 °C for 72 h and then cooled to room temperature. The resulting precipitate was washed with 0.1 M HNO_3 solution until pH value of 1–2 was reached. The final product was then collected by centrifugation and dried at 70 °C for 12 h in air. Ordered mesoporous carbon CMK-3 (pore-size: 3 to 5 nm, BEM: 1431 m^2 g^{-1}, produced by XF Nano, INC) was used as received.

Characterization: The scanning electron microscopy (SEM) was conducted on a JSM-6390 microscope of JEOL. Transmission electron microscopy (TEM) experiments were conducted on a JEOL 2011 microscope (Japan) operated at 200 kV. Powder X-ray diffraction (XRD) data for the prepared titanate nanowires was collected with a Bruker D4 Endeavor X-ray diffractometer using CuKa radiation. Argon sorption was conducted to assess porosity and surface area data of titanate nanowires using Quadrasorb *SI* Automated Surface Area and Pore Size Analyzer.

Electrochemical Measurements: Composite electrodes were used for electrochemical measurements. For $H_2Ti_6O_{13}$ composite electrode, a mixture containing 85 wt% of active material $H_2Ti_6O_{13}$, 10 wt% of acetylene black, and 5 wt% of polytetrafluoroethylene (PTFE) was well mixed and then pressed onto a nickel mesh which served as a current collector. The preparation of CMK-3 composite electrode was as same as that of $H_2Ti_6O_{13}$ composite electrode, whereas aluminium mesh was used as current collector. In these electrochemical measurements of composite electrodes, Li metal foil was used as the counter and reference electrode, and 1 M $LiPF_6$ dissolved in 1:1 v/v mixture of ethylene carbonate/diethyl carbonate (EC/DEC) was employed as the electrolyte. Cyclic voltammetry (CV) and charge-discharge tests were performed with a Solartron Instrument Model 1287 controlled by a computer. In these electrochemical measurements of supercapacitor, $H_2Ti_6O_{13}$ composite and CMK-3 composite electrode were used as negative electrode and positive electrode, respectively, using organic electrolyte (1 M $LiPF_6$ EC/DCE). In this asymmetric supercapacitor, the mass ratio of positive electrode/negative electrode was 4:1. In CV testing, the electrode surface was only about 0.25 cm^2, and the mass loading of active material is 1 mg cm^{-2}. The purpose of the CV test was to investigate the kinetic mechanism of $H_2Ti_6O_{13}$ nanowires. In order to reduce the negative affect from internal impedance (including the resistance from electrolyte and the resistance from wire and connecting point), it was better to reduce absolute current value of electrode. Thereby, small size thin film electrode was employed to study the kinetic mechanism of electrode material. In the charge/discharge test for the electrode of $H_2T_6O_{13}$ nanowires, the electrode surface was 1 cm^2, and the mass loading of active materials was 4 mg cm^{-2}. In the electrochemical performance investigation of CMK-3//$H_2Ti_6O_{13}$ asymmetric supercapacitor, the mass loading of positive electrode (CMK-3) and negative electrode ($H_2Ti_6O_{13}$) were 8 mg cm^{-2} and 2 mg cm^{-2}, respectively. Surfaces of positive electrode and negative electrode were all 1 cm^2. All of the energy density (Wh kg^{-1}) and power density (W kg^{-1}) values were only calculated based on the mass of electrode active materials (CMK-3 and $H_2Ti_6O_{13}$).

Supporting Information

Supporting Information is available from the Wiley Online Library or from the author.

Acknowledgements

The authors acknowledge funding support from the National Natural Science Foundation of China (21103025, 20925312, and 21173049), the State Key Basic Research Program of PRC (2011CB935903), and Shanghai Science & Technology Committee (10JC1401500, 08DZ2270500).

Received: March 19, 2012
Revised: June 22, 2012
Published online: August 3, 2012

[1] B. E. Conway, *Electrochemical Supercapacitors: Scientific Fundamentals and Technological Applications*, Kluwer Academic/Plenum Publishers, New York **1999**.
[2] P. Simon, Y. Gogotsi, *Nat. Mater.* **2008**, *7*, 845.
[3] A. Izadi-Najafabadi, S. Yasuda, K. Kobashi, T. Yamada, D. N. Futaba, H. Hatori, M. Yumura, S. Lijima, K. Hata, *Adv. Mater.* **2010**, *22*, E235.
[4] M. Hughes, G. Z. Chen, M. S. P. Shaffer, D. J. Fray, A. H. Windle, *Chem. Mater.* **2002**, *14*, 1610.
[5] W. Sugimoto, H. Iwata, Y. Yasunaga, Y. Murakami, Y. Takasu, *Angew. Chem. Int. Ed.* **2003**, *42*, 4092.
[6] C. C. Hu, W. C. Chen, K. H. Chang, *J. Electrochem. Soc.* **2004**, *151*, A281.
[7] Y. Wang, C. Y. Foo, T. K. Hoo, M. Ng, J.Y. Lin, *Chem. Eur. J.* **2010**, *16*, 3598.
[8] Z.-S. Wu, D.-W. Wang, W. C. Ren, J. P. Zhao, G. M. Zhou, F. Li, H. M. Cheng, *Adv. Funct. Mater.* **2010**, *20*, 3595.
[9] T.-S. Hyun, H. L. Tuller, D-Y. Youn, H. G. Kim, I. D. Kim, *J. Mater. Chem.* **2010**, *20*, 9172.
[10] C. Z. Yuan, L. Chen, B. Gao, L. H. Su, X. G. Zhang, *J. Mater. Chem.* **2009**, *19*, 246.
[11] Y.-M. Chen, J.-H. Cai, Y.-S. Huang, K.-Y. Lee, D.-S. Tsai, K.-K. Tiong, *Nanotechnology* **2011**, *22*, 355708.
[12] J. Zang, X. D. Li, *J. Mater. Chem.* **2011**, *21*, 10965.
[13] A. J. Roberts, R. C. T. Slade, *J. Mater. Chem.* **2010**, *20*, 3221.
[14] J. Yan, E. Khoo, A. Sumboja, P. S. Lee, *ACS Nano* **2010**, *4*, 4247.
[15] L Hu, W. Chen, X. Xie, N. Liu, Y. Yang, H. Wu, Y. Yao, M. Pasta, H. N. Alshareef, Y. Cui, *ACS Nano* **2011**, *5*, 8904.
[16] H. Y. Lee, J. B. Goodenough, *J. Solid State Chem.* **1999**, *148*, 81.
[17] D. W. Choi, G. E. Blomgren, P. N. Kumta, *Adv. Mater.* **2006**, *18*, 1178.
[18] Q. Lu, M. W. Lattanzi, Y. Chen, X. M. Kou, W. F. Li, X. Fan, K. M. Unruh, J. G. Chen, J. Q. Xiao, *Angew. Chem. Int. Ed.* **2011**, *50*, 6847.
[19] Y. G. Wang, Y. Y. Xia, *Electrochim. Acta* **2006**, *51*, 3223.
[20] J. P. Liu, J. Jiang, C. Cheng, H.X. Li, J. Zhang, H. Cong, H. J. Fan, *Adv. Mater.* **2011**, *23*, 2076.
[21] T. Y. Wei, C.-H. Chen, H.-C. Chien, S.-Y. Lu, C.-C. Hu, *Adv. Mater.* **2010**, *22*, 347.
[22] L. Cao, F. Xu, Y. Y. Liang, H. L. Li, *Adv. Mater.* **2004**, *16*, 1583.
[23] Y. G. Wang, H. Q. Li, Y. Y. Xia, *Adv. Mater.* **2006**, *18*, 2619.
[24] J. Akimoto, K. Chiaba, N. Kijima, H. Hayakawa, S. Hayashi, Y. Gotoh, Y. Idemoto, *J. Electrochem. Soc.* **2011**, *158*, A546.
[25] T. Brezesinski, J. Wang, S. H. Tolbert, B. Dunn, *Nat. Mater.* **2010**, *9*, 146.
[26] H. Lindström, S. Södergren, A. Solbrand, H. Rensmo, J. Hjelm, A. Hagfeldt, S.-E. Lidquist, *J. Phys. Chem. B* **1997**, *101*, 7717.
[27] A. J. Bard, L. R. Faulkner, *Electrochemical Methods Fundamentals and Applications*, 2nd ed., John Wiley, Inc, New York **2001**, Ch. 6, p. 233, 235.
[28] H. J. Liu, J. Wang, C. X. Wang, Y. Y. Xia, *Adv. Energy Mater.* **2011**, *1*, 1101.
[29] H. J. Liu, X. M. Wang, W. J. Cui, D. Y. Zhao, Y. Y. Xia, *J. Mater. Chem.* **2010**, *20*, 4223.
[30] H. Q. Li, R. L. Liu, D. Y. Zhao, Y. Y. Xia, *Carbon* **2007**, *45*, 2628.
[31] D. D. Zhou, H. J. Liu, Y. G. Wang, C. X. Wang, Y. Y. Xia, *J. Mater. Chem.* **2012**, *22*, 1937.
[32] Y. G. Wang, L. Yu, Y. Y. Xia, *J. Electrochem. Soc.* **2006**, *153*, A743.
[33] Y. G. Wang, Y. Y. Xia, *Electrochem. Commun.* **2005**, *7*, 1138.
[34] L. Cheng, H. J. Liu, J. J. Zhang, H. M. Xiong, Y. Y. Xia, *J. Electrochem. Soc.* **2006**, *153*, A1472.
[35] Z. J. Fan, J. Yan, T. Wei, L.J. Zhi, G. Q. Ning, T. Y. Li, F. Wei, *Adv. Funct. Mater.* **2011**, *21*, 2366.
[36] G. H. Yu, L. B. Hu, M. Vosgueritchian, H. L. Wang, X. Xie, J. R. McDonough, X. Cui, Y. Cui, Z. N. Bao, *Nano Lett.* **2011**, *11*, 2905.
[37] L. Demarconnay, E. Raymundo-Pinero, F. Béguin, *J. Power Socures* **2011**, *196*, 580.
[38] Q. Wang, Z. H. Wen, J. H. Li, *Adv. Funct. Mater.* **2006**, *16*, 2141.
[39] Z. Chen, V. Augustyn, J. Wen, Y. W. Zhang, M. Q. Shen, R. Dunn, Y. F. Lu, *Adv. Mater.* **2011**, *23*, 791.